Available online at www.sciencedirect.com
ScienceDirect
Ceramics International 36 (2010) 1633–1643
CERAMICS INTERNATIONAL
www.elsevier.com/locate/ceramint

Improvements in microstructural, mechanical, and biocompatibility properties of nano-sized hydroxyapatites doped with yttrium and fluoride

Burcin Basar [a], Aysen Tezcaner [a,b], Dilek Keskin [a,b], Zafer Evis [a,b,*]

[a] *Middle East Technical University, Department of Engineering Sciences, Ankara 06531, Turkey*
[b] *Middle East Technical University, Graduate Department of Biomedical Engineering, Ankara 06531, Turkey*

Received 17 December 2009; received in revised form 29 January 2010; accepted 20 February 2010
Available online 25 March 2010

Abstract

Hydroxyapatite was doped with Y^{3+} (2.5, 5 and 7.5 mol%) and F^- (2.5 mol%) ions (2.5YFHA, 5YFHA, 7.5YFHA, respectively) to compare its structural and mechanical properties and cellular response with pure-hydroxyapatite. No second phases were observed by X-ray diffraction spectra of 2.5YFHA. Doped hydroxyapatites had F^- bonds in addition to OH^- bonds. Hydroxyapatites sintered at 900 and 1100 °C were in nano-size. 7.5YFHA sintered at 1300 °C had the highest microhardness value. 2.5YFHA sintered at 1100 °C had the highest fracture toughness value. MTT viability assays showed high cell attachments on 2.5YFHA. Cell proliferation on 2.5YFHA and 5YFHA sintered at 1100 and 1300 °C was comparable with the control after 5-day culture. The highest ALP production and calcium deposition were observed on all hydroxyapatites sintered at 1100 °C. 2.5YFHA sintered at 1100 °C can be an alternative for hydroxyapatite in orthopedic applications.

Keywords: A. Sintering; B. X-ray methods; C. Hardness; D. Apatite; E. Biomedical applications

1. Introduction

Hydroxyapatite (HA, $Ca_{10}(PO_4)_6(OH)_2$) has been used as an implant material for bones and teeth due to its excellent biocompatibility to human hard tissues because it has similar structure with the mineral part of bone [1]. Nevertheless, its poor mechanical characteristics limit the applications of HA in load-bearing areas [2]. HA has been vastly applied in non-load-bearing fields such as ossicles in middle ear [1,2].

HA has Ca and P elements in its hexagonal structure. These elements are the same elements present in the inorganic parts of the bone and teeth. Due to the reason that its elemental composition consists of the same components, the host reaction is minimized. In fact, strong bonds are generated onto the surface between bone and implant material due to the high bioactivity of HA [3]. There have been many attempts to improve the various properties of synthetic HA [4–6]. Bone minerals are in nano-scale; emphasis has been directed on improving the properties of nano-sized HA.

Various ions have been added to nano-HA to enhance its biological, mechanical and chemical properties. For example, Ergun et al. investigated the structure of HA doped with Mg^{2+}, Zn^{2+}, Cd^{2+} and Y^{3+} ions [7]. They stated that lattice parameters and hexagonal unit volume of doped HA decreased due to the complete substitution of Y^{3+} in HA. Additionally, Webster et al., investigated the effect of divalent (Mg^{2+}, Zn^{2+}) and trivalent (Y^{3+}, In^{3+}, La^{3+}, Bi^{3+}) dopants on characteristics of HA pertinent to orthopedic and dental applications; it was an attempt to improve the properties of HA related to these applications [8].

In addition to cation dopants, fluoride doping is frequently used in order to improve thermal stability and biological properties of HA. Fluoride substituted in HA influences the physical and biological characteristics of HA. Fluoride in saliva and blood plasma is necessary for dental and skeletal development; fluoride is known to be very important in suppressing dental caries [9,10]. It was also noted to stimulate proliferation and differentiation of bone cells [11]. Moreover, it has been used in treatment of osteoporosis [12]. However, high concentration of fluoride ions may also inhibit the cell

* Corresponding author at: Middle East Technical University, Department of Engineering Sciences, 06531 Ankara, Turkey. Tel.: +90 312 210 4450; fax: +90 312 210 4462.
E-mail address: evis@metu.edu.tr (Z. Evis).

0272-8842/$36.00
doi:10.1016/j.ceramint.2010.02.033

proliferation by releasing Ca^{2+} ions in HA due to decreased solubility [13]. Addition to the reports that high concentrations of fluoride led to abnormal tissue growth [14], poor mechanical properties occurred at high amount of additions of fluoride into HA, but lower fluoride levels improved the mechanical properties of HA, such as hardness, fracture toughness, elastic modulus and brittleness [15]. Therefore, the optimum fluoride concentrations in HA for biomaterial applications were reported as 0.033–0.4 mol F^-/mol apatite by previous studies [13,16].

Yttrium and fluoride ions were separately substituted into HA in previous studies [13,16]. Co-substitution of yttrium and fluoride was attempted for the first time in this study. HA doped with Y^{3+} and F^- were synthesized by a precipitation method and sintered at 900, 1100 and 1300 °C for 1 h. Densities of the materials were determined by Archimedes technique. Sintered samples were investigated by X-ray diffraction (XRD) and Fourier transform infrared spectroscopy (FTIR) to determine the phases and bonds generated in the structure of pure and doped hydroxyapatite after sintering. Scanning electron microscopy (SEM) was used to calculate the grain sizes of the samples. For mechanical characterization, microhardness testing was performed. A human osteoblast-like cell line Saos-2 with characteristic osteoblastic traits was used for the in vitro cell culture tests. The cellular response towards doped HA was studied in terms of cell attachment, proliferation and differentiation (ALP production and calcium deposition).

2. Experimental procedure

Pure nano-HA was synthesized by precipitation method [17,18]. Calcium nitrate tetra hydrate ($Ca(NO_3)_2{\cdot}4H_2O$) and di-ammonium hydrogen phosphate ($(NH_4)_2HPO_4$) were mixed to obtain pure HA. 0.6 M $Ca(NO_3)_2{\cdot}4H_2O$ and 0.3 M $(NH_4)_2HPO_4$ was separately prepared in distilled water. The Ca/P ratio was kept 1.67 to obtain the correct stoichiometry of HA. Ammonia solution was added into both solutions to bring the pH to 11–12 level. Calcium nitrate solution was drop wise added into continuously stirring di-ammonium hydrogen phosphate solution. After 3 h of stirring, the mixture was heated until boiling in order to increase the reaction rate and it was left to stirring overnight. Then, the mixture was filtered by using a fine filter paper to obtain a wet cake. The wet cake was dried in the furnace at 200 °C for 24 h. After the drying, calcination was performed at 600 °C for half an hour. Next, the sintering was applied at 900, 1100 and 1300 °C for 1 h.

For doped HA, the main precursors were same. Additionally, yttrium nitrate and ammonium fluoride were used to obtain starting solutions. Yttrium nitrate was added into calcium nitrate solution in 2.5, 5 and 7.5 mol% of calcium nitrate. Ammonium fluoride was added into di-ammonium hydrogen phosphate solution in composition of 2.5 mol% of di-ammonium hydrogen phosphate. The same procedure was used in preparation of pure HA and doped HAs. The proportions of elements added were adjusted according to mole percentage of precursors. After the solutions were mixed, the products were stirred, filtered, calcined and sintered as in the preparation of pure HA. In this study, the designations of pure and doped HAs depending on the composition are summarized in Table 1.

The density (ρ) of the materials was measured by Archimedes method. Following formula was used to calculate the density of the samples [19]:

$$\text{Density } (\text{g/cm}^3) = \frac{Wt_{(\text{air})}}{Wt_{(\text{air})} - Wt_{(\text{water})}} \times \rho_{(\text{water})} \quad (1)$$

where $\rho_{(\text{water})}$ is the density of water. Theoretical density of the pure and doped HA was assumed to be same (3.156 g/cm^3).

Phases present in the samples were investigated by XRD using a Rigaku DMAX 2200 machine. XRD was performed on the samples with a Cu-Kα radiation at 40 kV/40 mA and samples were scanned from 20° to 60° in 2θ with a scan speed of 2.0°/min. Joint Committee on Powder Diffraction Standards (JCPDS) files were used for comparison with the positions of diffracted planes taken from XRD results; therefore, the phases in powders were determined. The hexagonal lattice parameters of hexagonal pure and doped HA were calculated by successive approximations [20]. In order to calculate the lattice parameter 'a' for the hexagonal crystal system of HA, the Bragg's equation was based. The following formula was used to calculate 'a_0' [20]:

$$a_0 = \left(\frac{\lambda}{2\sin\theta}\right)\sqrt{\left(\frac{4}{3}(h^2 + hk + k^2) + \left(\frac{a}{c}\right)^2 l^2\right)} \quad (2)$$

where a_0 is the calculated lattice constant; λ is X-ray wavelength; θ is the Bragg angle for corresponding (h k l); a/c is the last calculated ratio in successive approximation.

If the value of the term **DiacriticalGrave;DiacriticalGrave;** $(4/3)(h^2 + hk + k^2)''$ was larger than the value of the term **DiacriticalGrave;DiacriticalGrave;**$(\mathbf{a/c})^2\mathbf{l}^2$ for a reflection of (h k l), this formula was used to calculate a_0. Furthermore, if the

Table 1
Summary of sample designations, % relative densities and average grain sizes (determined from SEM image) of pure HA, 2.5YFHA, 5YFHA and 7.5YFHA sintered at 900, 1100 and 1300 °C.

Sample	Description	% Relative density			Average grain size (nm)		
		900 °C	1100 °C	1300 °C	900 °C	1100 °C	1300 °C
HA	Undoped HA	85.7	94.5	94.3	86.6	271.0	3487
2.5YFHA	2.5% Y^{3+}–2.5% F^--HA	97.2	99.2	98.9	82.6	224.0	2409
5YFHA	5% Y^{3+}–2.5% F^--HA	95.7	95.9	96.5	56.3	204.8	1832
7.5YFHA	7.5% Y^{3+}–2.5% F^--HA	92.8	95.3	98.2	51.4	200.7	1641

value of the term **DiacriticalGrave;DiacriticalGrave;h^2 + hk + k^2** was less than the value of "l^2", it was used to calculate c_0. To minimize the error caused by incorrect axial ratio, another formula was used to calculate c_0 [20]:

$$c_0 = \left(\frac{\lambda}{2\sin\theta}\right)\sqrt{\left(\frac{4}{3}\left(\frac{c}{a}\right)^2(h^2+hk+k^2)+l^2\right)} \quad (3)$$

The volume of the hexagonal unit cell of the materials was calculated according to the following formula:

$$V = 2.589 \cdot (a^2) \cdot c \quad (4)$$

where V (Å^3) is the volume of unit cell, a and c are the hexagonal lattice parameters in Angstroms.

FTIR spectra were used to identify the presence of OH^- and F^- bonds formed in the doped and undoped HA structure. The samples were first crushed in mortar and pestle. Ceramic powders and potassium bromide (KBr) were mixed with 1–300 weight ratio. The prepared powder mixture was cold pressed to obtain transparent pellets. The spectra records were performed from 1400 to 400 cm^{-1} using a 512 scan on FTIR spectrometer (Brukers IFS 66/S; Bruker Optics, Germany).

A JEOL JSM-6400 (JEOL Ltd., Japan) SEM at a voltage of 20 kV was used to examine the samples. Before the examination, the samples were first polished with SiC papers (Buehler Ltd., USA) from 240 to 1200 grit. Final polishing was performed with 1 μm monocrystalline diamond suspension (Buehler Ltd., USA) and the samples were finally etched with a 0.5 M HF acid for 2 min. At the end, they were coated with gold.

Grain size determination of the samples was performed using SEM images of pure and doped HAs sintered at 900, 1100 and 1300 °C. The intercept method was used with a 20 cm circumference circle to find out the grain sizes of HAs. Grain sizes from SEM images were determined using following formula [21]:

$$G_a = \frac{L}{N \times M} \quad (5)$$

where G_{av} is the average grain size; L is the circumference of the circle (20 cm); N is the number of intersections along circumference line, M is the magnification.

The microhardness of the samples was determined by a Vickers microhardness tester (HMV-2, Shimadzu, Japan). The sintered discs were used to determine the microhardness of the materials. A diamond indenter was applied with a load of 200 g for 20 s onto the surface of the discs. The diagonal indent shape formed after the indentation was measured to determine the microhardness of the samples. 20 measurements were performed on each sample. For the calculation, the following formula was used:

$$HV = 0.001854\frac{P}{d^2} \quad (6)$$

where HV is the Vickers hardness (GPa); P is the applied load (N); d is the diagonal indent length (mm).

Fracture toughness of the samples was determined according to the length of the cracks generated by the indentations applied during the microhardness test. Halfpenny shape cracks were formed after the microhardness measurements. When Halfpenny shaped cracks were generated, the Evans and Charles equation was used to calculate the fracture toughness [22]:

$$K_{1c} = 0.0824\frac{P}{C^{1.5}} \quad (7)$$

where P is the applied load (N) and C is the crack length (m).

In vitro cytotoxicity studies using Saos-2 cells (human osteosarcoma cell line) were performed to study the biocompatibility of pure and doped HA discs sintered at different temperatures. Pure and doped HA discs were sterilized at 200 °C for 2 h. All cell culture reagents were from Biochrom, Germany unless stated in the text.

MTT viability assay (Sigma, USA) was used to assess cell proliferation on pure and doped HA discs. 5×10^4 cells/disc were seeded on discs and cultivated in Dulbecco's modified Eagle medium (DMEM) supplemented with 10% fetal bovine serum (FBS) for 1, 3 and 5 days at 37 °C. Discs were then incubated with MTT for 4 h at 37 °C. After removal of MTT solution, formazan crystals inside cells were solubilized with dimethyl sulfoxide. Absorbance at 550 nm was measured with a μOuant™ microplate spectrophotometer (Biotek Instruments Inc., USA).

The attachment efficiency of Saos-2 cells on discs was determined by normalizing the absorbance readings with that of tissue culture polystyrene (TCPS). The cell attachment on TCPS (control surface) was taken as 100%.

The intracellular ALP activity was measured as a differentiation marker for osteoblastic cells to assess the differentiation state of the cells. 4×10^4 cells/disc were seeded on discs and were incubated in osteogenic differentiation medium (DMEM supplemented with 10% FBS, 1% penicillin–streptomycin, 0.1% sodium pyruvate, 50 μg/ml ascorbic acid, 10 mM β-glycerophosphate and 10^{-8} M dexamethasone) for 14 days. After 7 and 14 days of incubation, the cells on discs were frozen and thawed three times in 600 μl of 0.1% Triton X-100 (Sigma, USA) to disrupt cell membranes [23]. 20 μl aliquots of each cell lysate were added to 100 μl pNPP substrate solution (Sigma–Aldrich, Germany). After 15 min incubation at 37 °C, the absorbance of each sample was measured at 405 nm by using μOuant™ microplate spectrophotometer. *P*-Nitrophenol formed was determined from the calibration curve constructed in the range of 25–250 μM. ALP activity was normalized by protein content of the cell lysates. The specific ALP activity was expressed as nmol/mg protein/min. The protein content was determined by bicinchoninic acid (BCA) assay using the calibration curve for bovine serum albumin in the range of 0–1.2 mg/ml [24].

Calcium deposition by the cells was measured using calcium *o*-cresolphthalein complexone method to study the mineralization of matrix from the same cell lysates in ALP protocol [25]. 100 μl samples from cell lysates were added into 1 ml color reagent (25 mg *o*-cresolphthalein complexone powder (Sigma, USA) in 250 ml distilled water) and 1 ml buffer (37.8 ml

adenosine monophosphate (AMP) reagent in 250 ml distilled water, pH 10.7). After 15 min incubation the absorbance at 540 nm was measured. Calcium amount was determined from the calibration curve constructed in the range of 0–12.5 mg/dl. Calcium deposited by cells was normalized by the protein content of the cell lysate and was expressed as Ca/mg protein.

All data were expressed as mean ± standard deviation. One-way analysis of variance (ANOVA) was done with Tukey's Multiple Comparison Test for the post hoc pair wise comparisons using SPSS-15.0 Software (SPSS Inc., USA). Differences were considered as significant for $p \leq 0.05$.

3. Results

Percent relative densities of pure and doped HA sintered at 900, 1100 and 1300 °C are given in Table 1. General tendency was an increase in the density of all materials with increasing the sintering temperatures from 900 to 1300 °C. However, a significant difference in the values of densities of doped HAs with respect to temperatures was not observed. Indeed, very high densities (above 85%) for all samples were achieved after the sintering. It was seen in Table 1 that relative densities of dopes HAs was decreasing with increasing amounts of dopings. Moreover, 2.5YFHA sintered at 1100 °C exhibited the highest density.

The XRD results of HAs sintered at 1100 °C are shown in Fig. 1. Indeed XRD method was applied to all dried and sintered HAs at all sintering temperatures. However XRD graphs were closely identical with a few differences. Therefore, the most interesting results were inserted in this study. No second phases were observed in dried, calcined or sintered (900 °C) pure or doped HAs. The only dominant phase observed in XRD patterns was HA for all samples at all temperatures. Trace amounts of β-TCP were detected in XRD patterns of 5YFHA sintered at 1300 °C and 7.5YFHA sintered at 1100 and 1300 °C. Addition of impurities like Y^{3+} and F^{-} did not cause severe fluctuations in XRD patterns. All peaks closely matched with JCPDS file number 9-432 for HA; no other phases were observed in the patterns regardless of the temperature.

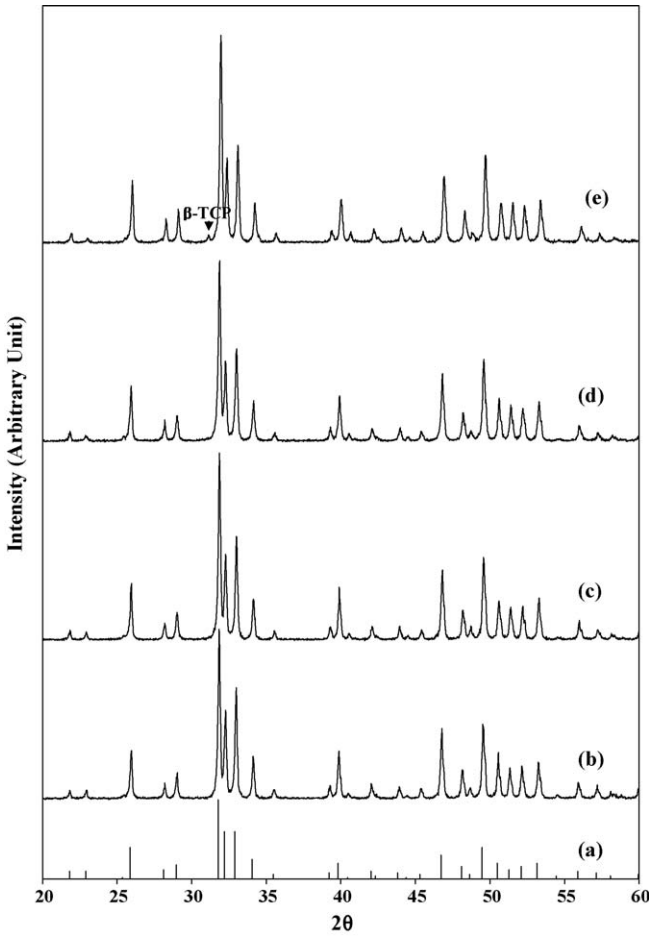

Fig. 1. XRD spectra of (a) standard HA (JCPDS#: 9-432), (b) pure HA, (c) 2.5YFHA, (d) 5YFHA and (e) 7.5YFHA sintered at 1100 °C.

Hexagonal lattice parameters and unit cell volumes of doped and undoped HA synthesized in this study are summarized in Table 2. As seen in the table, hexagonal lattice parameters '*a*' and '*c*' decreased for all materials at all temperatures. Naturally, unit cell volume of the lattices decreased. These reductions are more apparent for unit cell parameter "*a*", whereas the other parameter "*c*" is slightly altering with respect to "*a*".

Table 2
Hexagonal lattice parameters "*a*" and "*c*" and changes in lattice parameters and unit cells volumes for HA, 2.5YFHA, 5YFHA and 7.5YFHA sintered at 900, 1100 and 1300 °C.

Samples	Sintering temp.	*a* (Å)	*c* (Å)	Δ*a* (Å)	Δ*c* (Å)	Δ*V* (Å^3)
HA	900 °C	9.417	6.879	0.0000	0.0000	0.0000
2.5YFHA		9.400	6.869	−0.0163	−0.0097	−7.6997
5YFHA		9.396	6.865	−0.0208	−0.0144	−10.2626
7.5YFHA		9.394	6.865	−0.0227	−0.0141	−10.8004
HA	1100 °C	9.413	6.875	0.0000	0.0000	0.0000
2.5YFHA		9.406	6.874	−0.0077	−0.0011	−2.8201
5YFHA		9.408	6.877	−0.0057	0.0022	−1.3998
7.5YFHA		9.384	6.860	−0.0294	−0.0150	−13.2709
HA	1300 °C	9.412	6.876	0.0000	0.0000	0.0000
2.5YFHA		9.391	6.866	−0.0215	−0.0096	−9.3962
5YFHA		9.393	6.867	−0.0191	−0.0087	−8.4005
7.5YFHA		9.387	6.866	−0.0248	−0.0106	−10.7022

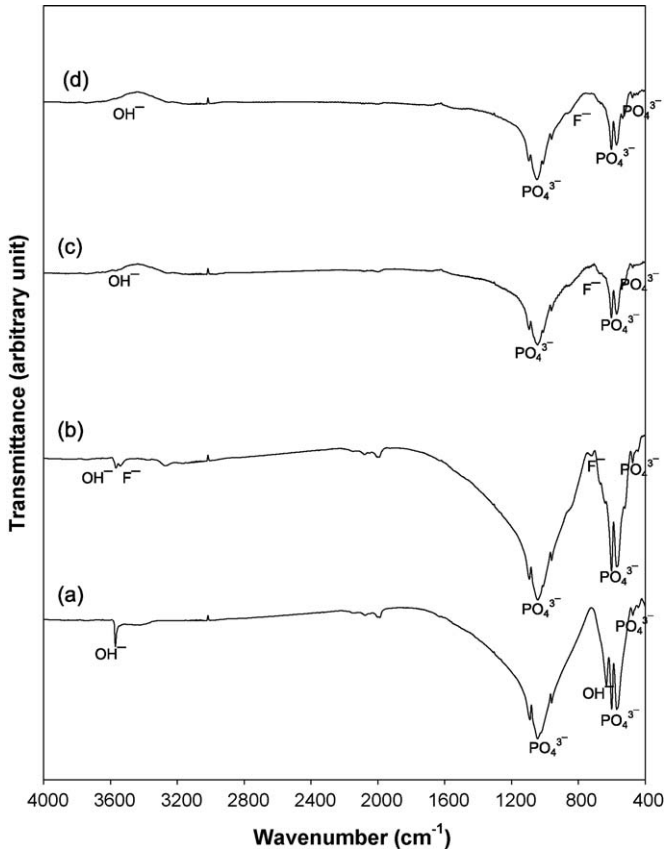

Fig. 2. FTIR spectra of (a) pure HA, (b) 2.5YFHA, (c) 5YFHA and (d) 7.5YFHA sintered at 1100 °C.

FTIR spectra of pure and doped HAs sintered at 1100 °C are represented in Fig. 2. Again here HAs sintered at only one temperature were given, because the other spectra were almost identical. For all samples, the main characteristic peaks of HA were observed.

As seen in SEM images in Fig. 3(a–l), temperature and amounts of dopants had important effects on grain sizes of the samples. SEM examinations revealed that HAs sintered at low temperatures below 1300 °C had more uniform microstructures and equiaxed fine grains. However, as the sintering temperature reached to 1300 °C, grain sizes exhibited severe growths. Nevertheless, it was observed that the addition of Y^{3+} and F^- ions into HA prevented the grain growth up to some extent. In Table 1, the effect of dopings and sintering temperatures on the grain sizes of pure and doped HAs are summarized. HAs sintered at 900 and 1100 °C were observed to be nano in size. But after the sintering at 1300 °C, very high increases in grain sizes were observed compared to other sintering temperatures.

The effect of temperature, density and dopings on microhardness was given in Figs. 4 and 5. The effect of co-substitutions of yttrium and fluoride dopings on microhardness was studied to optimize the amount of the additions. All pure HAs synthesized in this study had microhardness values around 4 GPa (Fig. 4). It can be noted that the lowest microhardness value of 3.3 GPa was measured for 5YFHA sintered at 900 °C, whereas the maximum microhardness value of 5.9 GPa was achieved for 7.5YFHA sintered at 1300 °C. Sintering effects on the mechanical properties of HA have been widely investigated.

In Fig. 6, fracture toughness of pure and doped HAs vs. sintering temperature are represented. The fracture toughness values attained with various temperatures and doping amounts ranged between 1.0 and 2.1 MPa $m^{1/2}$. The maximum fracture toughness of MPa $m^{1/2}$ was measured for 2.5YFHA sintered at 1100 °C (2.1 MPa $m^{1/2}$). The lowest fracture toughness value of 1.0 MPa $m^{1/2}$ was calculated for 5YFHA sintered at 900 °C.

Fig. 7 represents the attachment percentage of Saos-2 cells on pure and doped HAs after 24 h incubation. Cell attachment efficiency on pure and doped HAs was 80% or more (Fig. 7). There were no significant differences in cell attachment between doped HAs at 900 °C. The highest cell adhesion among all discs was observed on 2.5YFHA sintered at 1100 °C (103 ± 14%) which was statistically higher than pure HA and other doped HAs sintered at the same temperature.

The degree of proliferation of cells on pure and doped HAs sintered at different temperatures was investigated using MTT viability assay. The degree of proliferation of cells on discs sintered at 900 °C (Fig. 8a) was lower than on discs with same composition sintered at higher temperature (Fig. 8b and c). When sintering temperature was increased to 1100 °C, it was observed that cell proliferation on pure HA, 2.5YFHA, 5YFHA was comparable with control (Fig. 8b). However, OD readings for 7.5YFHA were statistically lower than on all other pure and doped HAs and control after 5 days of culture. Fig. 8c shows that cells also proliferated on all pure and doped HAs sintered at 1300 °C. Cell proliferation on 2.5YFHA was the highest among all pure and doped HAs after 5-day culture.

ALP activities of cells on pure and yttrium-fluoride doped HAs were studied at days 7 and 14 to investigate the effects of yttrium and fluoride doping sintered at different temperatures on differentiation state of the cells. As seen in Fig. 9a, ALP activity of Saos-2 cells on pure and doped HAs sintered at 900 °C increased with culturing time. ALP production of cells on doped HAs was numerically higher than those on pure HA. Significant increases in ALP activities were observed when the discs were sintered at 1100 °C in comparison to those for 900 °C (Fig. 9b). ALP activities of cells on pure and doped HAs increased with culture time except on 7.5YFHA. ALP activity measured on 7.5YFHA was significantly lower than on pure HA at day 14. Time dependent increase in the ALP production was also observed for pure HA and 2.5HYFA sintered at 1300 °C (Fig. 9c). Additionally, ALP production for these groups was significantly higher than the production measured for 5YFHA and 7.5YHA after 14 days of culturing. However, ALP activity measured on 5YFHA and 7.5YHA discs was still higher than those on the discs with same composition that were sintered at 900 °C. It was also found that pure and doped HAs sintered at 1100 °C, except 5YFHA, revealed a significant difference in ALP activity at day 14 from HAs sintered at two other sintering temperatures. Furthermore, ALP activities of cells on 5YFHA sintered at 1100 °C were found to be the highest among all dopant and sintering temperature groups.

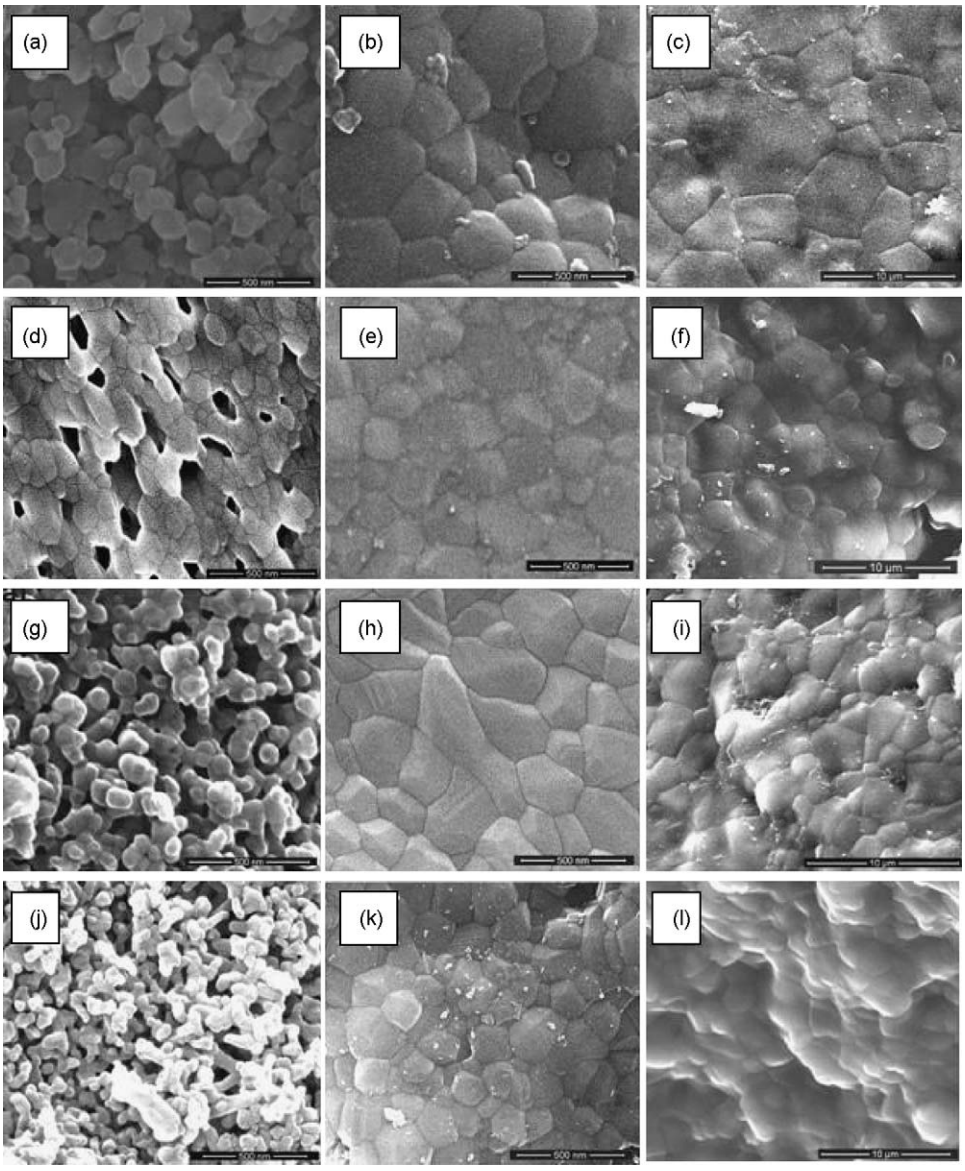

Fig. 3. SEM images of the samples studied in this study: pure HAs sintered at (a) 900 °C, (b) 1100 °C, (c) 1300 °C, 2.5YFHAs sintered at (d) 900 °C, (e) 1100 °C, (f) 1300 °C, 5YFHAs sintered at (g) 900 °C, (h) 1100 °C, (i) 1300 °C, 7.5YFHAs sintered at (j) 900 °C, (k) 1100 °C, (l) 1300 °C.

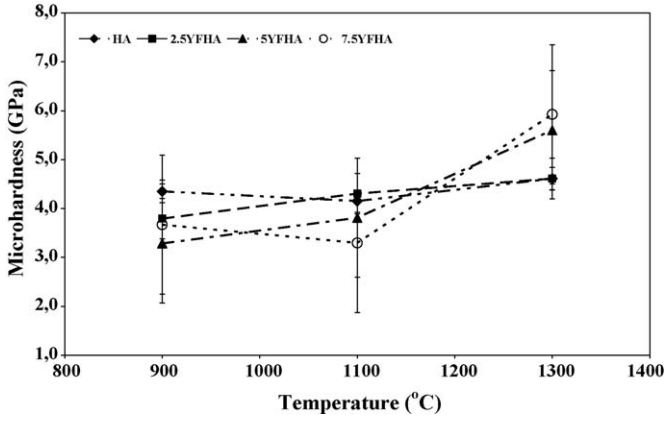

Fig. 4. The change in microhardness of pure and doped HAs with various compositions as a function of sintering temperature.

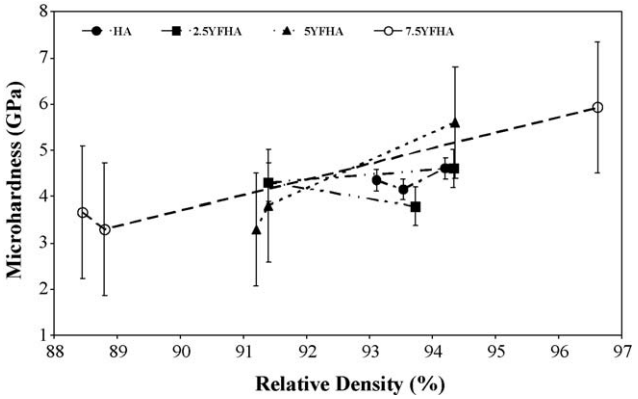

Fig. 5. The change in microhardness of pure and doped HAs with various compositions as a function of percent relative densities of HAs.

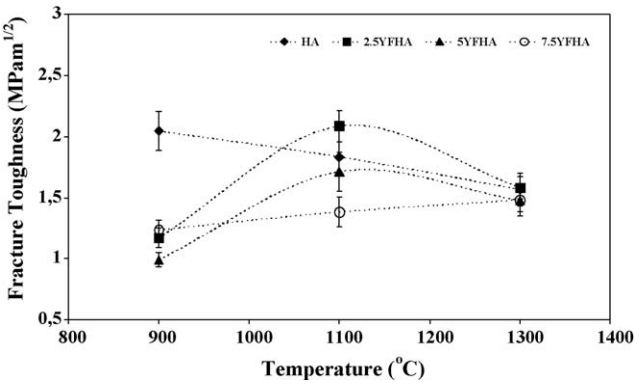

Fig. 6. The change in fracture toughness of pure and doped HAs with various compositions as a function of sintering temperature.

The extracellular calcium deposition of cells on pure and doped HA discs sintered at 3 different temperatures was studied after 7 and 14 days of incubation. With 900 °C sintering, a time dependent increase was observed for calcium amount deposited by cells on all discs (Fig. 10a). However, a significant increase in calcium deposited was only observed for 2.5YFHA and 7.5YFHA. As seen in Fig. 10a, Ca^{2+} contents for all HAs were similar at day 7. At day 14, pure HA, 5YFHA and 7.5YFHA had similar amounts of Ca^{2+} deposited by cells. However, calcium deposition on 2.5YFHA was significantly lower than those on other doped HAs. Fig. 10b represents extracellular calcium deposited by cells on pure and doped HAs discs sintered at 1100 °C. In general, at day 7, amount of calcium deposited on pure and doped HAs discs was statistically indifferent except 7.5YFHA which had higher calcium amount than other doped HAs. After 14 days, calcium deposition increased for all groups except 7.5HYFA. When 1300 °C was used for sintering, calcium deposition of cells on pure HA, 2.5YFHA and 7.5YFHA were similar at day 7 (Fig. 10c). No significant increase in the calcium amounts was observed with time for doped HAs. A decrease in the calcium amount at day 14 was observed for 5HYFA. Additionally, the calcium deposition on pure HA was significantly higher than on doped HAs at day 14.

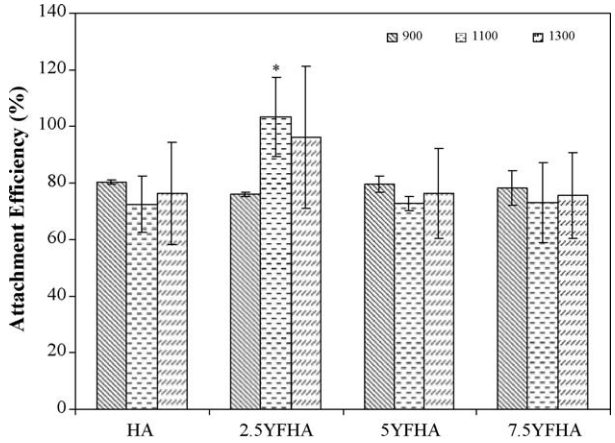

Fig. 7. Cell attachment on pure and doped HAs sintered at different temperatures after 24 h. *Statistically different from other discs sintered at 1100 °C.

The calcium deposition amounts on doped HAs sintered at 1300 °C were similar to the ones sintered at 1100 °C.

4. Discussion

In the ambient atmosphere, HA tends to decompose by the following reaction [26]:

$$Ca_{10}(PO_4)_6(OH)_2 \rightarrow 3Ca_3(PO_4)_2 + CaO + H_2O \quad (8)$$

Since the water is given off at the end of this reaction, pores are generated in the material. However, it was deduced that the addition of Y^{3+} and F^- ions into HA prevented this reaction to occur, because doping of HA with Y^{3+} and F^- ions resulted in a decrease in porosity with respect to pure HA, as seen in Table 1. On the other hand, sinterability of doped HAs seemed to become lower as the amount of yttrium ions increased. This could be resulted from formation of stronger bonding of yttrium and fluoride hindering the diffusion necessary for sintering. For these reasons, small amount of β-TCP was observed in the sample 7.5YFHA after the sintering at 1100 and 1300 °C.

There are two calcium sites (Ca(1) and Ca(2)) present in the hexagonal structure of the apatites. Out of 10 calcium ions, there are 4-Ca(1) and 6-Ca(2) ions present in a hexagonal unit cell [27]. Yttrium (Y^{3+}) and other rare-earths (Eu^{3+}, Nd^{3+}) have ionic radii close to that of Ca^{2+} ions. Therefore, they are easily accepted into the apatite lattice [28]. In this study, doping of Y^{3+} ions in the unit cell of HA probably substituted into the Ca(2) locations in the hexagonal unit cell. Because, it was previously shown that the trivalent ions (Nd^{3+}, La^{3+}) all substituted in to the Ca(2) sites in the apatites [29,30]. This could be one of the reasons why the density of the yttrium and fluoride doped HAs was higher than that of the pure HA.

Since the only phase determined in the structure of the materials by XRD was HA, except 5YFHA sintered at 1300 °C and 7.5YFHA sintered at 1100 and 1300 °C, the method used in synthesis of HA was successfully performed. For further investigation of the microstructures of HAs lattice parameters were determined. It was found that hexagonal lattice parameters of doped HAs were smaller than that of pure HA at all temperatures. Because ion sizes of both Y^{3+} and F^- are smaller than those of Ca^{2+} and OH^- ions, it is expectable that the addition of these ions resulted in the shrinkage of lattices. Ionic radii of Y^{3+} and Ca^{2+} ions are 0.9 and 1.0 Å, respectively [31]. The F^- and OH^- ions have ionic radii of 1.32 and 1.68 Å, respectively [32,33]. When the Y^{3+} ions were doped between 2.5 and 7.5%, there were about one-Y^{3+} ion substitution for approximately between 40 and 12 Ca^{2+} ions present in the structure. For example, there was almost one-Y^{3+} ion present in a hexagonal unit cell after the doping of 7.5% Y^{3+} ion into the apatite. The contradictions in lattice parameters are believed to be resulted mostly from F^- ions rather than Y^{3+} ions. Because the difference between ionic radii of OH^- and F^- ions is more significant than that between Y^{3+} and Ca^{2+} ions. Therefore, unit cell volume of 2.5YFHA was smaller than that of pure HA as seen in Table 2 because of the presence of added ions.

FTIR investigations showed that OH^- libration bands around 630 and 3571 cm^{-1} were only intense for pure HA.

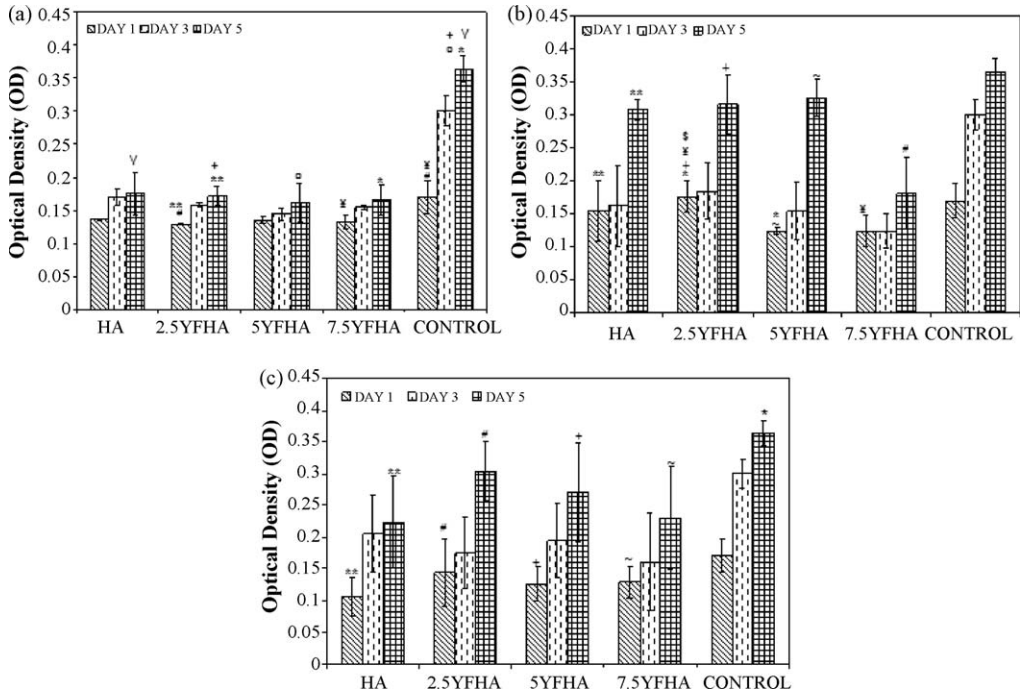

Fig. 8. Cell proliferation on pure and doped HAs discs sintered at (a) 900 °C, (b) 1100 °C, and (c) 1300 °C. Cells seeded on TCPS were used as control (significant differences between groups *, **, ¥, γ, ¤, +, **, ∼, #, $p < 0.05$).

Bands assigned to PO_4^{3-} group were around 962, 474, 1087 and 601 cm^{-1}. The patterns of doped HAs were similar to that of pure HA, except some additional F^- bands indicating substitutions of added ion with OH^- ions into HA. OH^- libration band at around 630 cm^{-1} which were clearly seen in pure HAs were erased or almost disappeared in the spectra of doped HAs. Moreover, as Ca/P ratio decreased from pure HA to 7.5YFHA, OH^- libration band at 630 cm^{-1} decreased in intensity. F^- bands at around 700 and 858 cm^{-1} appeared in the patterns of doped HAs as shown in Fig. 2. Partial substitution of OH^- ions by F^- was verified for the presence of the bands at 3545 and 3569 cm^{-1} for the doped HAs after the sintering at

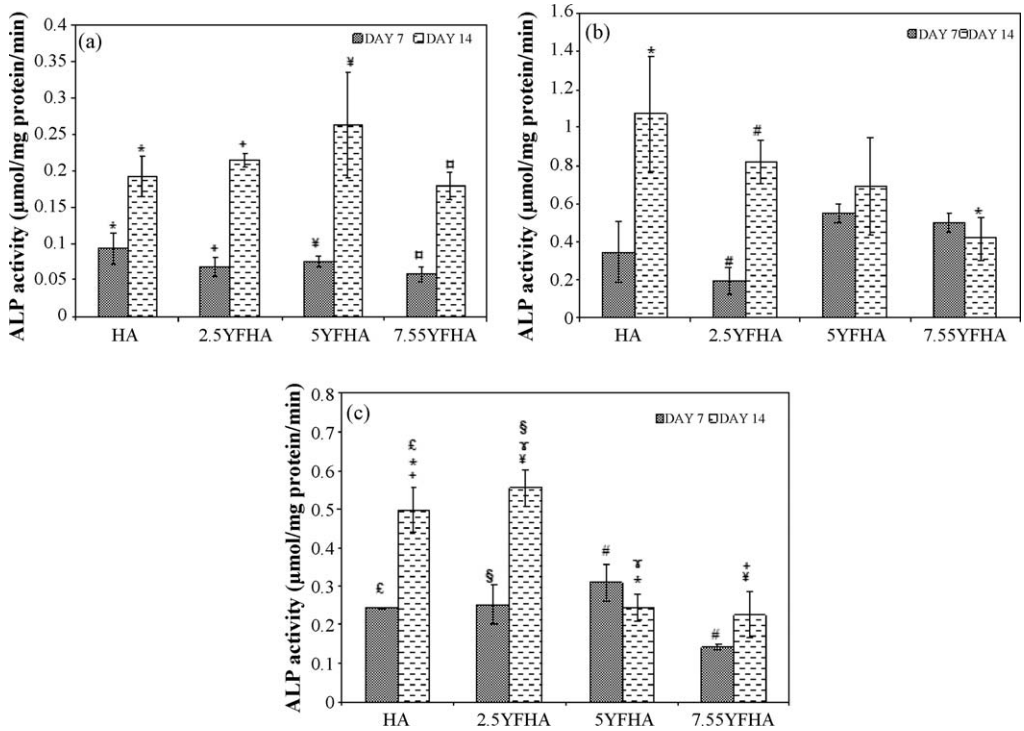

Fig. 9. ALP activity of cells on pure and doped HAs s sintered at (a) 900 °C, (b) 1100 °C, (c) 1300 °C incubated for 7 and 14 days (significant differences between groups *, +, ¥, ¤, #, £, §, ❣, $p < 0.05$).

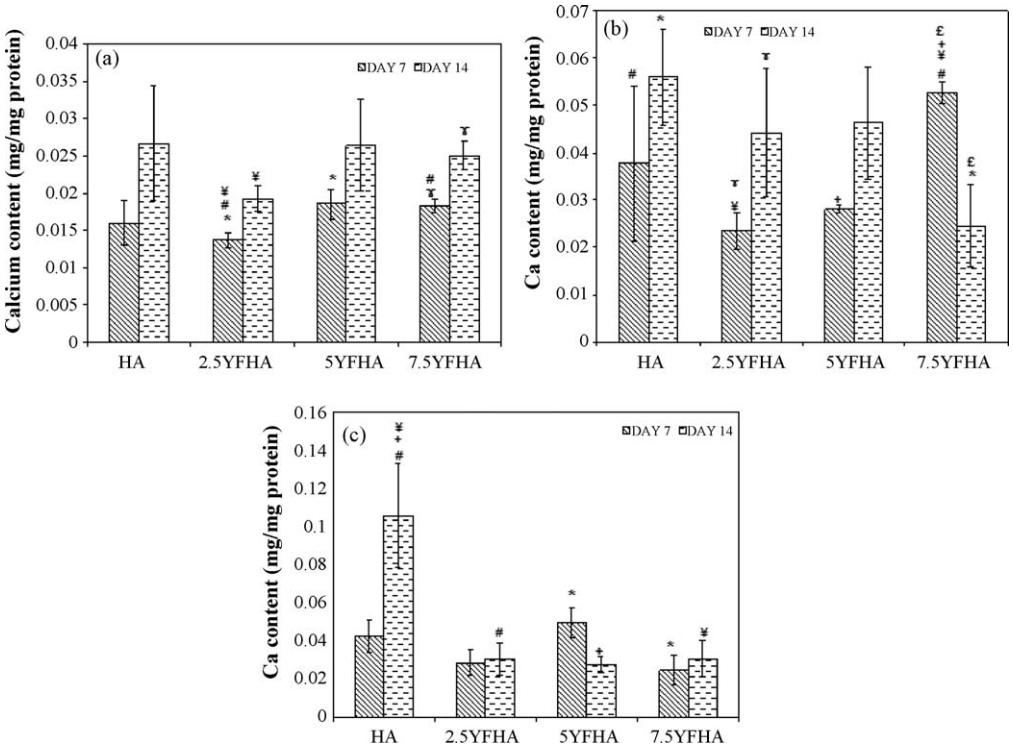

Fig. 10. Calcium content of cells on pure and doped HAs s sintered at (a) 900 °C, (b) 1100 °C, (c) 1300 °C incubated for 7 and 14 days (significant differences between groups *, #, ¥, +, £, ‡, $p < 0.05$).

900, 1100, and 1300 °C. The main characteristic absorbtion bands of HA were preserved with increasing the temperatures, only some additional bands showing the substitutions with ions in HA were added in the FTIR spectra.

Grain sizes were determined form SEM images of the materials. Pure HA had the largest grain size for all sintering temperatures compared to doped HAs. Decrease in grain sizes at the same sintering temperatures could be attributed to the dopings. Initially, the grain sizes increased slowly by a factor of between 2 and 4, when sintering temperature went to 1100 °C from 900 °C. However, when sintered at above 1100 °C, the grain sizes increased by a factor of between 8 and 12. Similarly, Ramesh et al. [34] reported that the average grain size increase by a factor of more than 7, from 0.88 μm at 1150 °C to 7.13 μm at 1300 °C. It was demonstrated that since higher temperatures were able to provide the activation energy of HA for grain growth, when sintered above 1250 °C, considerable grain growth (by a factor of about 6) occurred compared to other samples sintered at lower temperatures [35]. In the present study, it was clearly seen that increasing temperature caused the grain size of pure HA to grow 40-fold from 86.6 nm at 900 °C to 3487 nm at 1300 °C. For doped HAs, the same trends were observed with temperature changes. As the amount of doped ions increased, the grain size decreased for HAs sintered at the same temperature. Accordingly, the material with the smallest grain size was 7.5YFHA with 51.4 nm sintered at 900 °C due to low sintering temperature and high amount of dopings. With the addition of Y^{3+} and F^{-} ions, nano-sized HA was obtained even at 1100 °C. Previous reports announced that the grain sizes of HA doped with fluoride ions increased with increasing degree of fluoridation [36,37], while addition of yttrium into HA led to decrease in the grain sizes of the materials [7,13]. Therefore, decreases in grain sizes measured in this study could be attributed to yttrium dopings into HA. It can also be concluded that nano-sized HAs were successfully produced at the end of the sinterings, except at 1300 °C.

In previous studies, it has been reported that Vickers microhardness of pure HA ranged from 1.17 to 6.86 GPa for various sintering temperatures [35,38]. Microhardness values of doped HAs sintered at 900 °C were about between 3.3 and 3.8 GPa in this study. The similar pattern was also observed for doped HAs sintered at 1100 °C; almost all doped HAs, except 2.5YFHA, had lower microhardness than pure HA. Only the microhardness of 2.5YFHA was slightly higher than that of pure HA at 1100 °C. However, doped HAs sintered at 1300 °C had higher microhardness values than pure HA sintered at that temperature. As the amount of dopings increased, the microhardness values increased after the sintering at 1300 °C (4.6, 5.6, and 5.9 GPa). Besides the amount of dopants, there must have been a correlation between hardness and the relative density and the grain size at various temperatures (Fig. 5). At similar densities (93–94.5%), 5YFHA seemed to have greater microhardness than that of pure HA and 2.5YFHA. The increase in yttrium amount resulted in greater hardness along with increasing density. 7.5YFHA with a highest density (96.6%) had the greatest microhardness value with a grain size smaller than other HAs.

In literature, fracture toughness values for pure HA sintered at various temperatures was found to vary in the range of 0.96–1.45 MPa $m^{1/2}$ [35,39]. Therefore, HAs synthesized in this

study had higher fracture toughness values compared to those in literature. Correlated to the previous graph of microhardness vs. temperature, it was shown that harder materials had lower fracture toughness, naturally. As the sintering temperatures were increased, the fracture toughness of pure HA became lower due to the increase in relative density. However, the fracture toughness of Y^{3+} and F^- doped HAs sintered at 900 and 1100 °C increased with the increasing sintering temperatures. Additions into pure HA prevented the fracture toughness from severe decrease, which was resulting from increasing temperatures. However, at the higher sintering temperatures such as 1300 °C, lower fracture toughness values were determined than those at 900 and 1100 °C, probably due to the severe grain growths in HAs sintered at 1300 °C.

It was also noted that the grain sizes decreased with increasing proportions of dopants for all sintering temperatures, as seen in Table 1. In addition to the lower degree of porosity, the grain sizes of pure and doped HAs sintered at 1300 °C increased abruptly, which could be interpreted that the high relative density and larger grain size might have been the governing parameters concerning the microhardness values. The highest grain sizes were obtained by HAs sintered at 1300 °C, with increasing amount of yttrium. Grain sizes at this temperature were decreasing while microhardness values increased, indicating that increasing yttrium resulted in contributions to grain size and microhardness.

The adhesion of Saos-2 cells on all discs was high suggesting that their surface properties were suitable for cellular attachment. MTT viability assay suggested that sintering temperatures and amounts of dopings affected the proliferation of the cells (Fig. 8). In literature, minimum levels of doping have also been reported for promoting cell adhesion and proliferation [13,16,40]. Nano-sized bioceramics were known to be better for cell adhesion and proliferation compared to micron-sized bioceramics [24,41]. In the current study, it was observed that cells highly adhered and proliferated even on larger grain-sized pure HAs or when doped with 2.5 or 5% yttrium together with 2.5% fluoride. This could be interpreted as a more pronounced effect of yttrium and fluoride ions dopings compared to grain size.

ALP activities of cells on HAs also changed according to the amount of yttrium doping and sintering temperature. ALP activities of cells on 2.5YFHA sintered at 1100 °C were the highest among all dopant and sintering temperature groups. In parallel with literature [8,41], lower amounts of yttrium led to increase ALP activities. The amount of calcium deposited on pure and doped HA sintered at 1100 °C was about twofold higher than the discs with same composition sintered at 900 °C (Fig. 10) in agreement with higher proliferation (Fig. 8) and ALP activities (Fig. 9). The highest calcium deposition and ALP activities were observed on discs sintered at 1100 °C. Webster et al. [8] reported that yttrium doped HA did not stimulate the calcium deposition of osteoblastic cells after 7 and 21 days of incubation. They also stated that ALP activity was not enhanced by yttrium doping into HA compared to undoped HA [8]. In agreement with this finding, fluoride and yttrium doping of HAs did not improve ALP activity and calcium deposition of cells. These findings support that sintering temperature changes the surface properties of pure and doped HA and affect the cell response to the biomaterial.

5. Conclusions

Hydroxyapatite doped with Y^{3+} (2.5, 5 and 7.5 mol%) and F^- (2.5 mol%) ions were synthesized, sintered and characterized by microstructural and mechanical methods. High densifications were observed in spite of increased grain sizes when the sintering temperature was increased from 1100 to 1300 °C. Almost no second phase formations were encountered in the XRD patterns of doped HAs sintered for all sintering temperatures. Addition of yttrium and fluoride ions into pure HA led to decrease in lattice parameters and unit cell volumes of doped HAs. FTIR analysis showed that the Y^{3+} and F^- doped HAs had F^- and OH^- bonds after the sintering. SEM images showed that HAs sintered at 900 and 1100 °C were in nano-size, addition of dopings prevented the grain growth and resulted in smaller grain sizes. Sample doped with 2.5% Y^{3+} and 2.5% F^- ions had the optimum microhardness and fracture toughness values. Lowest Y^{3+} and 2.5 mol% F^- doped HA sintered at 1100 °C had the highest cell attachment while its proliferation and bone specific differentiation markers were comparable with pure HA. We conclude that 2.5YFHA sintered at 1100 °C has a potential for consideration as an alternative for HAs in orthopedic applications. Further investigations should be focused on this material in order to understand the all mechanisms for future biomechanical and orthopedic applications.

Acknowledgement

This study was financially supported by the grant of The Scientific and Technological Research Council of Turkey (Project number: 105M271).

References

[1] L.L. Hench, Bioceramics: from concept to clinic, J. Am. Ceram. Soc. 74 (1991) 1487–1510.
[2] K. DeGroot, C. DePutter, P. Smitt, A. Driessen, Mechanical failure of artificial teeth made of dense calcium hydroxylapatite, Sci. Ceram. 11 (1981) 433–437.
[3] R.H. Doremus, Review: bioceramics, J. Mater. Sci. 27 (1992) 285–297.
[4] K. Ioku, M. Yoshimura, S. Somiya, Microstructure and mechanical properties of hydroxyapatite ceramics with zirconia dispersion prepared by post-sintering, Biomaterials 11 (1990) 57–61.
[5] K. Uematsu, M. Takagi, T. Honda, N. Uchida, K. Saito, Transparent hydroxyapatite prepared by hot isostatic pressing of filter cake, J. Am. Ceram. Soc. 72 (1989) 1476–1478.
[6] G.D. With, H.J.A.V. Dijk, N. Hattu, K. Prijs, Preparation, microstructure and mechanical properties of dense polycrystalline hydroxyapatite, J. Mater. Sci. 16 (1981) 1592–1598.
[7] C. Ergun, T.J. Webster, R. Bizios, R.H. Doremus, Hydroxylapatite with substituted magnesium, zinc, cadmium, and yttrium. I. Structure and microstructure, J. Biomed. Mater. Res. 59 (2002) 305–311.
[8] T.J. Webster, E.A. Massa-Schlueter, J.L. Smith, E.B. Slamovich, Osteoblast response to hydroxyapatite doped with divalent and trivalent cations, Biomaterials 25 (2004) 2111–2121.

[9] H.W. Kim, Y.M. Kong, Y.H. Koh, H.E. Kim, H.M. Kim, J.S. Ko, Pressureless sintering and mechanical and biological properties of fluor-hydroxyapatite composites with zirconia, J. Am. Ceram. Soc. 86 (2003) 2019–2026.
[10] O. Nakade, H. Koyama, J. Arai, H. Ariji, J. Takad, T. Kaku, Stimulation by low concentrations of fluoride of the proliferation and alkaline phosphatase activity of human dental pulp cells in vitro, Arch. Oral Biol. 44 (1999) 89–92.
[11] J.R. Farley, J.E. Wergedal, D.J. Baylink, Fluoride directly stimulates proliferation and alkaline phosphatase activity of bone-forming cells, Science 222 (1983) 330–332.
[12] M. Sivakumar, I. Manjubala, Preparation of hydroxyapatite/fluorapatite zirconia composites using Indian corals for biomedical applications, Mater. Lett. 50 (2001) 199–205.
[13] K. Cheng, W. Weng, H. Wang, S. Zhang, In vitro behavior of osteoblast-like cells on fluoridated hydroxyapatite coatings, Biomaterials 26 (2005) 6288–6295.
[14] J.M. Guise, A. Mc Cormack, P.A. Anderson, A.F. Tencer, Effect of controlled local release of sodium fluoride on trabecular bone, J. Orthop. Res. 10 (1992) 588–595.
[15] K.A. Gross, L.M. Rodriguez-Lorenzo, Sintered hydroxyfluorapatites. Part II: Mechanical properties of solid solutions determined by microindentation, Biomaterials 25 (2004) 1385–1394.
[16] H. Kim, Y. Kong, J.C. Knowles, Fluor-hydroxyapatite sol–gel coating on titanium substrate for hard tissue implants, Biomaterials 25 (2004) 3351–3358.
[17] Z. Evis, Al^{3+} doped nano hydroxyapatites and their sintering characteristics, J. Ceram. Soc. Jpn. 114 (2006) 1001–1004.
[18] Z. Evis, Reactions in hydroxylapatite–zirconia composites, Ceram. Int. 33 (2007) 987–991.
[19] H. Kuwahara, N. Mazaki, M. Takahashi, T. Watanabe, X. Yang, T. Aizawa, Mater. Sci. Eng. A 319–321 (2001) 687–691.
[20] B.D. Cullity, Elements of X-ray Diffraction, second edition, Addison-Wesley, MA, USA, 1978.
[21] J.E. Hilliard, Estimating grain size by the intercept method, Metal Prog. Data Sheet (1964) 99–102.
[22] C.B. Ponton, R.D. Rawlings, Vickers indentation fracture toughness test. Part I: Review of literature and formulation of standardized indentation toughness equation, Mater. Sci. Technol. 5 (1989) 865–872.
[23] C. Ratisoontorn, M.L. Seto, K.M. Broughton, M.L. Cunningham, In vitro differentiation profile of osteoblasts derived from patients with Saethre–Chotzen syndrome, Bone 36 (2005) 627–634.
[24] T.J. Webster, C. Ergun, R.H. Doremus, R.W. Siegel, R. Bizios, Enhanced functions of osteoblasts on nanophase ceramics, Biomaterials 21 (2000) 1803–1810.
[25] H.J. Gitelman, An improved automated procedure for the determination of calcium in biological specimens, Anal. Biochem. 18 (1967) 521–531.
[26] Z. Evis, R.H. Doremus, Effect of YF_3 on hot-pressed hydroxyapatite and monoclinic zirconia composites, Mater. Chem. Phys. 105 (2007) 76–79.
[27] A.S. Posner, A. Perloff, A.F. Diorio, Refinement of the hydroxyapatite structure, Acta Crystallogr. 11 (1958) 308–309.
[28] P.L. Roeder, D. MacArthur, X.-P. Ma, G.R. Palmer, A.N. Mariano, Cathodoluminescence and microprobe study of rare-earth elements in apatite, Am. Miner. 72 (1987) 801–811.
[29] R.C. Ohlmann, K.B. Steinbruegge, R. Mazelsky, Spectroscopic and laser characteristics of neodymium-doped calcium fluorophosphate, Appl. Opt. 7 (1968) 905–914.
[30] L.W. Schroeder, M. Mathew, Cation ordering in $Ca_2La_8(SiO_4)_6O_2$, J. Solid State Chem. 26 (1978) 383–387.
[31] R.D. Shannon, Revised effective ionic radii and systematic studies of inter atomic distances in halides and chaleogenides, Acta Crystallogr. Sect. A 32 (1976) 751–767.
[32] T.S.B. Narasaraju, D.E. Phebe, Some physico-chemical aspects of hydroxylapatite, J. Mater. Sci. 31 (1996) 1–21.
[33] R.A. Young, Implications of atomic substitutions and other structural details in apatites, J. Dent. Res. 53 (1974) 193–203.
[34] S. Ramesh, C.Y. Tan, I. Sopyan, M. Hamdi, W.D. Teng, Consolidation of nanocrystalline hydroxyapatite powder, Sci. Technol. Adv. Mater. 8 (2007) 124–130.
[35] G. Muralithran, S. Ramesh, The effects of sintering temperature on the properties of hydroxyapatite, Ceram. Int. 26 (2000) 221–230.
[36] K.A. Gross, L.M. Rodriguez-Lorenzo, Sintered hydroxyfluorapatites. Part I: Sintering ability of precipitated solid solution powders, Biomaterials 25 (2004) 1375–1384.
[37] E.J. Lee, H.W. Kim, H.E. Kim, Biocompatibility of fluor-hydroxyapatite bioceramics, J. Am. Ceram. Soc. 88 (2005) 1309–1311.
[38] B. Cengiz, Y. Gokce, N. Yildiz, Z. Aktas, A. Calimli, Synthesis and characterization of hydroxyapatite nanoparticles, Colloids Surf. A Physicochem. Eng. Aspects 322 (2008) 29–33.
[39] S. Ramesh, C.Y. Tan, S.B. Bhaduri, W.D. Teng, Rapid densification of nanocrystalline hydroxyapatite for biomedical applications, Ceram. Int. 33 (2007) 1363–1367.
[40] M. Sato, M.A. Sambito, A. Aslani, N.M. Kalkhoran, E.B. Slamovich, T.J. Webster, Increased osteoblast functions on undoped and yttrium-doped nanocrystalline hydroxyapatite coatings on titanium, Biomaterials 27 (2006) 2358–2369.
[41] T.J. Webster, R.W. Siegel, R. Bizios, Osteoblast adhesion on nanophase ceramics, Biomaterials 20 (1999) 1221–1227.